CHALMERS
UNIVERSITY OF TECHNOLOGY

Integrating Reconfigurable Intelligent Surfaces (RISs) into Indoor D-MIMO Networks for 6G

Downloaded from: https://research.chalmers.se, 2025-01-19 19:45 UTC

Citation for the original published paper (version of record):
Vayal Parambath, A., Flordelis, J., Madapathage Don, C. et al (2024). Integrating Reconfigurable Intelligent Surfaces (RISs) into Indoor D-MIMO Networks for 6G. 2024 IEEE 100th Vehicular Technology Conference (VTC2024-Fall).
http://dx.doi.org/10.1109/VTC2024-Fall63153.2024.10757793

N.B. When citing this work, cite the original published paper.

© 2024 IEEE. Personal use of this material is permitted. Permission from IEEE must be obtained for all other uses, in any current or future media, including reprinting/republishing this material for advertising or promotional purposes, or reuse of any copyrighted component of this work in other works.

(article starts on next page)

Integrating Reconfigurable Intelligent Surfaces (RISs) into Indoor D-MIMO Networks for 6G

Akshay Vayal Parambath[1], Jose Flordelis[2], Charitha Madapatha[1], Fredrik Rusek[2], Erik Bengtsson[2], Tommy Svensson[1]

[1] Chalmers University of Technology, Gothenburg, Sweden - (vayal, charitha, tommy.svensson)@chalmers.se
[2] Sony Research Center, Lund, Sweden - (jose.flordelis, fredrik.x.rusek, erik.bengtsson)@sony.com

***Abstract*—In this paper, we study integration strategies for reconfigurable intelligent surfaces (RISs) in distributed MIMO (D-MIMO) systems as one of the promising techniques for evolving 5G networks and beyond (6G). The scalability of D-MIMO systems to large networks in a practically feasible way is challenging. The exploitation of cost-effective and energy-efficient dynamic access point (AP) clustering techniques and densification enablers is crucial for such systems to sustain the required level of performance and reliability while mitigating the environmental and economic challenges related to future network operations. RIS is well regarded as a low-cost, rapidly deployable, energy-efficient candidate offering extra diversity in the spatial domain. This work explores RIS-aided multi-AP systems attaining certain prescribed key performance indicators (KPIs) while considering the energy consumption in the system.**

We concentrate on indoor use cases with large user equipment (UE) populations where the service coverage is low due to the high obstacle density. To that end, we propose dynamic user-centric AP clustering and RIS placement techniques adapted for serving multi-user indoor systems. Here, we use an alternating optimization method as a sub-optimal solution for RIS phase-shift configuration, keeping the computation complexity low. We show that the integration of RISs in D-MIMO systems is an attractive approach to enhance energy efficiency and provide the scalability required in 5G and beyond (6G).

***Index Terms*—D-MIMO, RIS, user-centric AP clustering, energy efficiency, service coverage probability, 5G, 6G, Reconfigurable intelligent surface.**

I. Introduction

The exponential growth and advancement in the field of wireless communications look forward to a future with a highly reliable and energy-efficient network. Initially, most of the research in wireless communication mainly aimed to provide a consistent and high quality of service (QoS) to its users, which has led to an energy efficiency trade-off from the system power consumption perspective. Thus, it became important to consider an energy-efficient technology capable of tackling this trade-off and thereby promoting sustainability in the upcoming generation of wireless networks.

The present multiple input multiple output (MIMO) networks are planned to be replaced by distributed MIMO (D-MIMO) networks that serve users by multiple access points (APs) instead of a single AP as in the MIMO network. Serving UEs with multiple distributed APs creates macro-diversity and leads to better data rates, reliability, and service coverage [1]. Even though the D-MIMO network is capable of providiing the above-mentioned performance improvement, the users in the network still suffer from a lack of service coverage due to high blockage especially in an indoor scenario due to the presence of multiple stationary and mobile obstacles [2]. Thus, the use of network extenders was found necessary to expand the coverage. Repeaters capable of redirecting the signal from APs to unreachable users by beamforming using amplify-and-forward were the initial choice of solution to this problem. These repeaters require a particular backhaul (BH) and access link to enable their beamforming capability and thus contribute to higher overall network energy consumption if deployed abundantly in a lower coverage area [1]. Thus, it became crucial to come up with an energy-efficient alternative that is capable of resolving the network coverage issue. Reconfigurable intelligent surfaces (RIS), which combine the technologies and properties of metasurface materials with multi-antenna techniques to reshape the radio propagation environment can play a pivotal role as an alternative solution to resolve such issues.

RIS is a planar meshed surface with multiple passive reflective surfaces attached to each grid, which can coordinately align its phases using a controller and perform beamforming. Thus, like repeaters, RIS will also require a control link but not any particular BH and access link with additional capabilities to support the beamforming [1]. RISs can be deployed densely in a network due to their low energy consumption. Also, the passive nature of the elements in RIS allow them to be coated to any surface without hassle, making its deployment faster. Hence, deploying RIS in an indoor D-MIMO network can efficiently solve the service coverage issue while being sustainable.

In this paper, we study the performance improvement gained by integrating RIS to an indoor D-MIMO system with high UE density. We also focus on identifying optimal AP cluster sizes and strategies to use RIS for serving the UEs in the above system. Furthermore, we investigate the potential of RIS to replace an AP in a multi-AP serving scenario like D-MIMO.

The structure of the rest of the paper is as follows. In section II, we discuss the system model where we investigate the deployment strategies, modeling of the RIS, channel model, alternating optimization algorithm for joint precoding, associ-

This work was supported by the European Commission through the Horizon Europe/JU SNS project Hexa-X-II (Grant Agreement no. 101095759).

ation strategies, and scheduler model. In section III, a comparative study is performed between D-MIMO systems with and without RIS integration for the best AP cluster sizes to analyze the benefits and future use cases of RIS. In this section, we also provide performance parameter analysis of signal-to-interference-plus-noise ratio (SINR), energy efficiency, and service coverage probability for the RIS-assisted D-MIMO system w.r.t. the transmit power of the AP, and number of RIS elements to validate its influence in the performance of the system model. Finally, in section IV, conclusions are drawn from the previous section and our future works are also discussed.

II. System Model

As shown in Fig. 1, we consider a two-tier heterogeneous (HetNet) indoor D-MIMO network. The size of the indoor environment is 300 m x 150 m where APs with N_{TX} antennas and gain G_{TX} are uniformly deployed at a height h_{AP}. The operational bandwidth (B) of the system is chosen as 100 MHz while carrier frequency (f_{c}) is chosen as 4 GHz (sub-6 GHz frequency range). We model the user equipment (UE) distribution by a finite homogeneous Poisson point process (FHPPP) with user density Λ, which suits well to model the random number of UEs distributed inside a finite region. Here, the UEs are considered to have N_{RX} antennas with gain G_{RX}.

The RIS is modeled as a mesh square grid model consisting of $N \times N$ elements each having a gain G_{RIS} and dimensions $\lambda/2 \times \lambda/2$ m^2. Each element is l-bit reconfigurable and thus has 2^l combinations of phase shifts for redirecting the incident signal to the desired direction. To find the best locations for deploying RIS within each cell in the traditional D-MIMO model, we analyze the average service coverage probability received by the UEs corresponding to all possible locations within each cell for multiple UE realizations. The RISs are then deployed at those positions that give the maximum service coverage probability for the UEs in the system.

A. Channel model

The 3GPP TR 38.901 line-of-sight (LoS) probability ($\mathrm{Pr}_{\mathrm{LoS}}$) model for indoor hotspot (InH) is used for checking the LoS availability between the AP and UE based on the 2D-Euclidean distance d_{2D} between them [3] as shown below.

$$\mathrm{Pr}_{\mathrm{LoS}}(d_{\mathrm{2D}}) = \begin{cases} 1, \text{ if } d_{\mathrm{2D}} \leq 1.2 \text{ m}; \\ \exp(\frac{-(d_{\mathrm{2D}}-1.2)}{4.7}), \text{ if } 1.2 \text{ m} < d_{\mathrm{2D}} < 6.5 \text{ m}; \\ \exp(\frac{-(d_{\mathrm{2D}}-6.5)}{32.6}) \cdot 0.32, \text{ if } d_{\mathrm{2D}} \geq 6.5 \text{ m}. \end{cases} \tag{1}$$

We use Rayleigh and Rician small-scale fading, while 3GPP TR 38.901 InH pathloss model is used to characterize the pathloss between the AP and UE based on the 3D-Euclidean distance d_{3D} [4] [5]. The LoS pathloss (δ_{LoS}) and NLoS pathloss (δ_{NLoS}) have separate formulae as shown below.

$$\delta_{\mathrm{LoS}}(d_{\mathrm{3D}}) = 32.4 + 17.3\log_{10}(d_{\mathrm{3D}}) + 20\log_{10}(f_{\mathrm{c}}) + \varepsilon_{\mathrm{LoS}}, \tag{2}$$

$$\begin{aligned} \delta_{\mathrm{NLoS}}(d_{\mathrm{3D}}) = &\max(\delta_{\mathrm{LoS}}(d_{\mathrm{3D}}), (38.3\log_{10}(d_{\mathrm{3D}}) \\ &+ 17.3 + 24.9\log_{10}(f_{\mathrm{c}}))) + \varepsilon_{\mathrm{NLoS}}. \end{aligned} \tag{3}$$

Here, $\varepsilon_{\mathrm{LoS}}$ and $\varepsilon_{\mathrm{NLoS}}$ represent the shadow fading in the LoS and NLoS paths respectively, which can be represented as a log-normal distribution with standard deviations values σ_{LoS} = 3 dB and σ_{NLoS} = 8.03 dB, respectively.

B. Alternating optimization algorithm for joint precoding

An alternating optimization algorithm for joint precoding as proposed in [6] is utilized to perform codebook-based beamforming for transmission in the downlink (DL). The above-mentioned algorithm is designed for a narrow-band system and therefore this algorithm serves as a foundation for developing a new algorithm to support a wide-band system. The pseudo-code of the algorithm for the wide-band system that is developed is shown in Algorithm 1. Aligning the phase of RIS towards a particular UE requires channel state information (CSI). In this research, we assume that CSI is already known to the transmitter for simplifying the problem formulation and analysis of the RIS-assisted D-MIMO system [7].

Algorithm 1 Alternating optimization of joint precoding for maximization of received power at UE for a wide-band system

repeat for $\kappa = 1, \ldots, W$ sub-carriers
  Initialize $w[\kappa]$, $q_1[\kappa]$, and $q_2[\kappa]$ to feasible values
  repeat for n iterations
    $g_w = G[\kappa]^{\mathrm{H}} w[\kappa]$ and $h_q = H_1[\kappa]q_1[\kappa] + H_2[\kappa]q_2[\kappa]$;
    Set $\Phi_n[\kappa] = -\angle g_w(n) h_q(n), \forall$ n $= 1, \ldots,$N;
    Phase correction, $\theta = \angle w[\kappa]^{\mathrm{H}} R_2[\kappa] q_2[\kappa]$;
    $A_1[\kappa] = R_1[\kappa]$; $A_2[\kappa] = (G[\kappa]\Phi[\kappa]H_2[\kappa]e^{-j\theta}) + R_2[\kappa]$;
    $A[\kappa] = A_1[\kappa] + A_2[\kappa]$;
    Perform SVD($A_1[\kappa]$) and SVD($A_2[\kappa]$) to obtain updated $q_1[\kappa]$ and $q_2[\kappa]$ as right unitary matrices;
    Perform SVD($A[\kappa]$) to obtain updated $w[\kappa]$ as left unitary matrix;
  until convergence;
  $P_r[\kappa] = \mid (w[\kappa]^{\mathrm{H}} A_1[\kappa] q_1[\kappa]) + (w[\kappa]^{\mathrm{H}} A_2[\kappa] q_2[\kappa]) \mid^2$
until end;
Perform greedy-algorithm to determine $q_1[\kappa_{opt}]$, $q_2[\kappa_{opt}]$, $w[\kappa_{opt}]$, and $\Phi[\kappa_{opt}]$ corresponding to κ_{opt} which provide $P_r[\kappa]_{max}$;
Utilize $q_1[\kappa_{opt}]$, $q_2[\kappa_{opt}]$, $w[\kappa_{opt}]$, and $\Phi[\kappa_{opt}]$ to re-calculate $P_r[\kappa]$ $\forall$ κ;

Here, for simplicity, without the loss of generality compared to a larger AP cluster serving scenario, we consider that 2 APs are serving each UE simultaneously, and 1 RIS supports coordinated serving. The channels $R_1^{'}[\kappa]$ and $R_2^{'}[\kappa]$ represent the channel between AP$_1$-UE and AP$_2$-UE corresponding to the sub-carrier κ respectively. Moreover, the channels $H_1^{'}[\kappa]$, $H_2^{'}[\kappa]$, and $G^{'}[\kappa]$ represent the channel between AP$_1$-RIS, AP$_2$-RIS, and RIS-UE respectively corresponding to the sub-carrier κ. Here, the channels are modeled as Rician or Rayleigh channels based on the availability of the LoS. Each channel has its corresponding effect on the channel gain G and pathloss δ between its transmitter and receiver end. For the Rician channel, the LoS component is modeled such that

it is influenced by a pair of the array response vector at AP (υ_{TX}), UE (υ_{RX}), or RIS (υ_{RIS}) end to include the effect of its respective phase variation to the channel to make the channel more realistic. The resultant direct channels from the two APs are denoted as $R_1[\kappa]$ and $R_2[\kappa]$ and the resultant channel between AP_1-RIS, AP_2-RIS, and RIS-UE are denoted as $H_1[\kappa]$, $H_2[\kappa]$, and $G[\kappa]$ respectively. The phase shift matrix of the RIS w.r.t. the sub-carrier κ is represented as $\Phi[\kappa]$, which holds phase shift values $\Phi_{\mathrm{n}}[\kappa]$ for $n = 1, \ldots, N$ on its diagonal, such that $\Phi[\kappa] = \mathrm{diag}(e^{j\Phi_1[\kappa]}, \ldots, e^{j\Phi_N[\kappa]})$. Here we implicitly assume G_{RIS} = 4 dB. The vectors $q_1[\kappa]$ and $q_2[\kappa]$ are used to represent the unit-norm precoder at AP_1 and AP_2 respectively for the sub-carrier κ. Furthermore, $w[\kappa]$ represents the unit-norm combiner at UE w.r.t. the sub-carrier κ. The precoders and combiner are of length N_{TX} and N_{RX} respectively. The precoded and combined channels are denoted as h_q and g_w, respectively.

In this model, the channel from AP_2 is considered to suffer from a larger pathloss than from AP_1 based on the AP selection in terms of pathloss between AP-UE. Hence, AP_2 requires additional assistance by RIS with its phase-shift optimized w.r.t. AP_2 and the UE that is being served. Firstly, we initialize $q_1[\kappa]$, $q_2[\kappa]$, and $w[\kappa]$ with feasible values and proceed to maximize $\mid w[\kappa]^{\mathrm{H}} G[\kappa]\Phi[\kappa]H_2[\kappa]q_2[\kappa] \mid^2$ and $\mid w[\kappa]^{\mathrm{H}} R_1[\kappa]q_1[\kappa] \mid^2 + \mid w[\kappa]^{\mathrm{H}} R_2[\kappa]q_2[\kappa] \mid^2$ by alternatively optimizing $\Phi[\kappa]$. Later, we repeat the same process vice-versa by fixing the obtained $\Phi[\kappa]$ and optimize $q_1[\kappa]$, $q_2[\kappa]$, and $w[\kappa]$. Here, singular value decomposition (SVD) is applied to the combined channel consisting of the direct channel and the channel via RIS to extract the unitary matrix representing the $q_1[\kappa]$, $q_2[\kappa]$, and $w[\kappa]$ at each step. The process is repeated for multiple iterations until convergence of the objective function.

The signals received by the UE through the above paths get coherently combined at the UE to obtain the power $|w[\kappa]^{\mathrm{H}} G[\kappa]\Phi[\kappa]H_1[\kappa]q_1[\kappa] + w[\kappa]^{\mathrm{H}} R_1[\kappa]q_1[\kappa] + w[\kappa]^{\mathrm{H}} G[\kappa]\Phi[\kappa]H_2[\kappa]q_2[\kappa] + w[\kappa]^{\mathrm{H}} R_2[\kappa]q_2[\kappa] \mid^2$ at subcarrier κ. This process is repeated for all the W sub-carriers and its corresponding received power at target UE $P_r[\kappa]$ is calculated. Utilizing this $P_r[\kappa]$, we perform greedy-algorithm to determine the optimal sub-carrier κ_{opt} that provides the maximum received power $P_r[\kappa]_{max}$. Afterwards, the $q_1[\kappa_{opt}]$, $q_2[\kappa_{opt}]$, $w[\kappa_{opt}]$, and $\Phi[\kappa_{opt}]$ corresponding to κ_{opt} are used to re-calculate the $P_r[\kappa]$ values. Here, we make an assumption that the channel remains consistent across all sub-carriers of the wide-band channel considering that any variation between the channels among the sub-carriers is negligible i.e., all sub-carriers of H, G, R. This same algorithm can be scaled for a larger serving AP cluster size ζ_{AP}, by combining the channels from each AP while alternatively optimizing its corresponding q, w, and Φ.

C. Association and scheduler model

It is crucial to create an association strategy-based model for efficient working of the system model. Here, we use the uniform clustering scheme (UCS) [8], to allocate the available resources uniformly among all the APs present in the system. Furthermore, we use a queue-based scheduling scheme (QSS) [8], which is responsible for assigning the APs and RIS for serving UEs in a particular timeslot t by assigning an availability status to each AP and RIS based on the maximum possible UEs it can simultaneously serve.

The QSS utilizes a UE-centric AP clustering approach [9] wherein each UE initially selects, from the available APs, a master AP. Here we chose to select the AP with the least pathloss. The master AP checks whether the number of available APs, including itself, and RISs in a particular timeslot is at least equal to the number of APs (p) and RISs (s) required to serve the UE. If this condition is satisfied, the master AP selects, to coordinately serve the UE, the p APs with the best channel condition. It then selects s RISs that can be associated with those APs having the worst channel channel condition among the serving APs. This selection of RIS is based on the availability of RIS. A distance constraint is also added for AP cluster selection to avoid the selection of far away APs that cannot serve the UE efficiently. An example model of D-MIMO serving a UE using AP cluster-size 4 and 1 RIS is illustrated in Fig. 1.

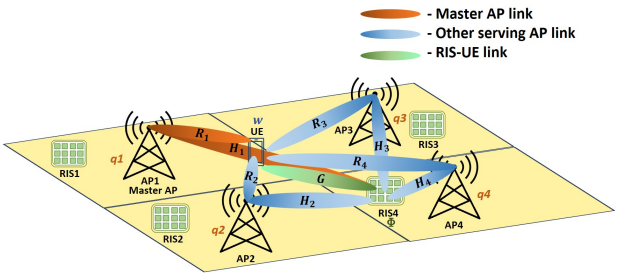

Fig. 1: RIS integrated D-MIMO system model representing a 4 AP cluster and 1 RIS serving UE scenarios.

This selection of APs and RIS by the UEs makes the selection process UE-centric instead of having a predefined serving APs and RIS based on the coverage area. If the master AP is unable to find the minimum required APs and RIS for serving a UE, this UE gets served in a later timeslot. This strategy of serving UEs ensures that, in the end, all the M UEs in the network are served fairly.

D. Performance metrics

We use the SINR (γ), data rate (R), energy efficiency (η), and service coverage probability (χ) to study the performance of different systems. The SINR γ_k observed at the k^{th} UE from the serving APs and RIS is given by the below equation.

$$\gamma_k = \frac{P_k}{I_k + \sigma_k^2}, \tag{4}$$

where σ_k^2 represents the noise power, P_k is the dominant signal power and I_k represents the cumulative interference power. The data rate R_k received by the k^{th} UE for a defined bandwidth B can be calculated using the Shannon-Hartley theorem. Moreover, the service coverage probability χ_k of the

k^{th} UE validates whether the received data rate (R_k) satisfies a minimum threshold data rate (R_{th}) [10]:

$$\chi_k = \begin{cases} 1, & \text{if } R_k \geq R_{\text{th}}; \\ 0, & \text{if } R_k < R_{\text{th}}. \end{cases} \tag{5}$$

The energy efficiency η_k measures the rate at which data can be sent per power consumption unit. The power consumption depends on various factors, including the transmit power P_{T}, the inverse of the transmit amplifier efficiency ξ, and the static power consumption of the whole system P_{c}. The energy efficiency while serving the k^{th} UE can be expressed as below [11].

$$\eta_k = \frac{R_k}{\xi P_{\text{T}} + P_{\text{c}}}. \tag{6}$$

The static power consumption can be further expressed as a combination of static losses, $P_{\text{AP}_{\text{static}}}$ at the AP, $P_{\text{UE}_{\text{static}}}$ at the UE, P_{b} at each RIS element [12], and P_{CB} at the RIS controller board [13] as shown below.

$$P_{\text{c}} = P_{\text{AP}_{\text{static}}} + P_{\text{UE}_{\text{static}}} + P_{\text{CB}} + (N_{\text{RIS}} \cdot P_{\text{b}}). \tag{7}$$

III. Simulation Results and Discussions

The system model described in section II is considered for simulation with the system parameters given in Table I.

TABLE I: System parameters.

Parameters	**Value**
f_{c}, B, κ	4 GHz, 100 MHz, 10
P_{T}	25 dBm
$P_{\text{AP}_{\text{static}}}$, $P_{\text{UE}_{\text{static}}}$, P_{b}, P_{CB}	9 dBW, 10 dBm, 0.01 dBm, 4.8 W
Noise figure (F_{UE})	10 dB
σ_{LoS} and σ_{NLoS}	3 dB and 8.03 dB
N_{TX} and N_{RX}	4 and 1
G_{TX}, G_{RX}, G_{RIS}	5 dB, 2 dB, 4 dB
Height of AP (h_{AP}) and UE (h_{UE})	2.5 m and 1.5 m
Height of RIS (h_{RIS})	2 m
Number of RIS elements (N_{RIS})	128
R_{th}	100 Mbps

In the simulations, 18 APs are deployed uniformly, and 100 UEs are randomly distributed over the area of deployment using FHPPP, and these UE locations were fixed during the analysis. The best RIS locations were identified by analyzing the average service coverage probability of the UEs for different locations of 18 RISs with one RIS in each of the 50 m $\times$ 50 m square grid in the total deployment area for 500 independent realizations of UEs. Here, the average service coverage probability values were determined for each position of all the 18 RISs. Utilizing these identified best positions that provide high service coverage probability, one RIS is deployed in each square grid in a fixed pattern with a constraint that each RIS is controlled by the AP in its corresponding square grid.

The applied analysis process consists of four stages: A) Comparing the SINR CDFs of conventional D-MIMO systems with different AP cluster sizes (ζ_{AP}) in order to determine the optimal ζ_{AP} values; B) Using the identified best three ζ_{AP} values, comparing the SINR CDFs of D-MIMO systems with and without integrated RIS to determine the significance of RIS in performance improvement; C) Analyzing the SINR CDFs in the RIS-assisted D-MIMO systems corresponding to the best three ζ_{AP} values for two different P_{T} values to study the influence of P_{T}; and D), E) analyzing the energy efficiency η and the service coverage probability χ of the RIS-integrated D-MIMO system by varying N_{RIS} to understand its corresponding variation patterns in terms of N_{RIS}.

A. Analysis of optimal AP cluster size of D-MIMO

The SINR of the UEs in a D-MIMO system is analyzed for AP cluster sizes between 1 and 6 to determine the optimal cluster size. The system with ζ_{AP} = 1 represents a MIMO system, and the systems with ζ_{AP} values from 2 to 6 represent D-MIMO systems. The systems with different ζ_{AP} and its corresponding median SINR (γ_{median}) values are given in Table II.

TABLE II: Median SINR of the UEs, in dB, versus AP cluster size.

ζ_{AP}	1	2	3	4	5	6
γ_{median} (dB)	32.04	36.65	42.65	43.60	44.02	42.29

From Table II, it can be observed that the median UE SINR shows a consistent trend as we scale the ζ_{AP} value from 1 to 3. The reason is that the intended received power at the UEs is dominant in comparison to the effective interference and noise at the served UEs. By contrast, γ_{median} increases only slightly when moving beyond ζ_{AP} = 3. Between ζ_{AP} = 3 and ζ_{AP} = 5, the improvement rate is dropping as the intended received power at the UEs is only enough to balance the resultant interference and noise. For the D-MIMO system with ζ_{AP} = 6, the γ_{median} value is dropping drastically and becomes lower than that of a D-MIMO system with ζ_{AP} = 3 due to the dominance of effective interference and noise at the served UEs. Thus, increasing ζ_{AP} beyond a certain threshold value does not help. From these results, it can be concluded that 2 and 3 are the best choices of ζ_{AP} for our D-MIMO setup.

B. Enhancement of D-MIMO performance with RIS integration w.r.t. different AP cluster sizes

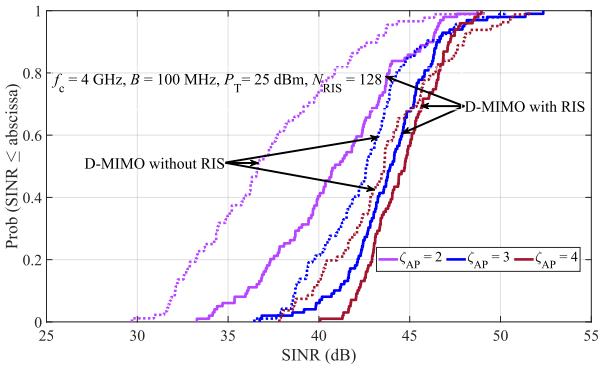

Fig. 2: SINR CDF comparison between D-MIMO systems with and without RIS for AP cluster sizes i) 2 APs, ii) 3 APs, and iii) 4 APs.

This analysis is performed to study the improvement in SINR at the UEs for the D-MIMO system with the integration of RIS. In this analysis, the D-MIMO system is analyzed for

the best three AP cluster sizes, i.e., $\zeta_{\mathrm{AP}} \in \{2, 3, 4\}$, obtained in the previous section. To this system, we integrate one RIS with N_{RIS} elements for serving each UE. Here, the RIS phase-shift is optimized to support the AP with a high pathloss. The SINR CDF at the UEs for the above system models were simulated for the above three ζ_{AP} values and compared with that of the conventional D-MIMO system. The corresponding simulation results are shown in Fig. 2.

Additional coordination with one RIS per served UE leads to a significant improvement of γ_{median} by 4.5 dB, 1.3 dB, and 1.1 dB for the ζ_{AP} values 2, 3, and 4, respectively. The improvement is especially notable for the case $\zeta_{\mathrm{AP}} = 2$. The fall in the enhancement rate of the RIS-assisted D-MIMO system observed for $\zeta_{\mathrm{AP}} = 3$ and 4 is due to the increases in the interference from the non-serving APs and RIS at the served UEs as ζ_{AP} increases. Furthermore, it can be observed that the γ_{median} corresponding to RIS-assisted D-MIMO system with ζ_{AP} = 3 outperforms the traditional D-MIMO system with ζ_{AP} = 4, which shows the potential of RIS in replacing the conventional D-MIMO system with a larger ζ_{AP} by a RIS-integrated D-MIMO system with a comparatively smaller ζ_{AP} value. The above results illustrate the SINR enhancement capability of RIS when deployed in a conventional D-MIMO system.

C. Performance analysis of different AP cluster sizes w.r.t. transmit power of AP for RIS-assisted D-MIMO system

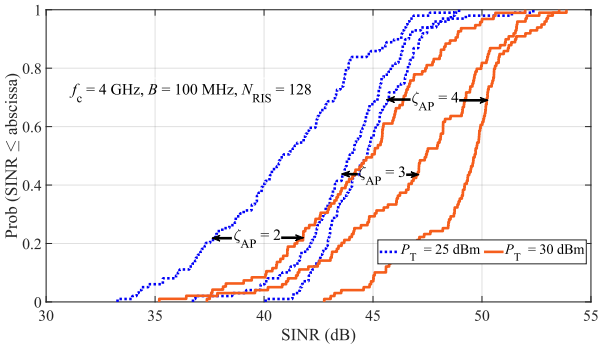

Fig. 3: SINR CDF comparison between different AP cluster sizes for transmit powers i) P_{T} = 25 dBm, and ii) P_{T} = 30 dBm with N_{RIS} = 128.

In this section, we analyze the CDF of the SINR at the UEs for $\zeta_{\mathrm{AP}} = 2$, 3, and 4 for the RIS-integrated D-MIMO system corresponding to P_{T} values of 25 dBm and 30 dBm. This analysis is performed to determine the influence of P_{T} on the UEs' SINR. The corresponding results are shown in Fig. 3. It can be observed that, when the P_{T} value is increased by 5 dBm, there is a significantly large rise in γ_{median} by 4 dB, 3.5 dB, and 5 dB corresponding to ζ_{AP} values 2, 3, and 4, respectively. This shows the influence of P_{T} over γ_{median}. Also, a consistent improvement in the γ_{median} can be seen for all three cases when P_{T} is increased by 5 dBm. This was found lacking in the scenario with P_{T} = 25 dBm. Furthermore, the γ_{median} gap between case i) case ii) increased by 0.5 dB but the γ_{median} gap between case ii) case iii) rose by 0.5 dB as we increased P_{T} by 5 dBm. These results show the trade-off between the γ and P_{T}. Also, it can be concluded that, a good improvement in γ_{median} at UEs is obtained when we increase the P_{T} by 5 dBm.

D. Energy efficiency analysis of RIS-integrated D-MIMO system

In this analysis, the average energy efficiency η of UEs present in the RIS-integrated MIMO (scenario (a) ζ_{AP} = 1) and D-MIMO system (scenario (b) ζ_{AP} = 2 and scenario (c) ζ_{AP} = 3) were analyzed by varying N_{RIS} over a range of 1 to 256 to study its extent of influence over η. Other than P_{T}, the static power consumption of AP, UE, RIS element, and RIS control board are also considered while analyzing η. The analysis is performed for three P_{b} values which include i) 0.01 dBm corresponding to the ideal passive RIS element, ii) 5 dBm, and iii) 10 dBm corresponding to a practical passive RIS element. The results for the above 3 cases corresponding to both the systems are shown in Fig. 4.

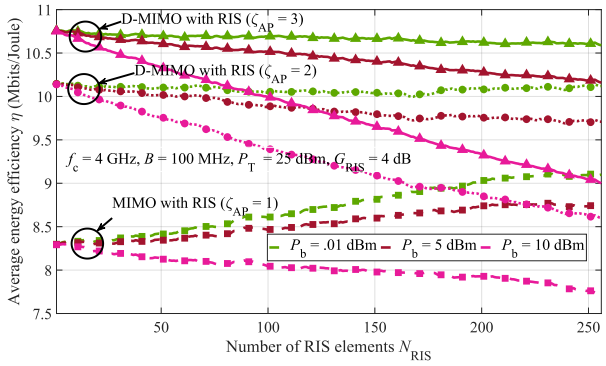

Fig. 4: Energy efficiency analysis w.r.t. the number of RIS elements for RIS-integrated MIMO and D-MIMO models.

The energy efficiency of the conventional MIMO system and D-MIMO system with ζ_{AP} values 2 and 3 were observed to be 8.06 Mbps/J, 10.01 Mbps/J, and 10.65 Mbps/J, respectively. These values were observed to be improved with the integration of RIS to these systems. In the case of scenario a) and b), it can be observed that η values show an increasing trend over the N_{RIS} range for case i) of P_{b}. However, the increasing rate is dropping significantly from scenario a) to b) because the received data rate (R) at UE is dominant to the overall power consumption of the system (P_{tot}) in scenario a) but R at UE is just enough to compensate P_{tot} in scenario b). The same factor resulted in having an almost similar improvement value of η over the N_{RIS} range for scenario c) corresponding to case i). This shows the influence of P_{b} on η for the RIS-assisted D-MIMO system.

It can be noticed that all the scenarios show a declining rate of η corresponding to case iii) with the drop rate rising from scenario a) to c). However, the η values show a good improvement of 1.85 Mbps/J in scenario b) compared to scenario a) but the improvement is reduced to 0.62 in scenario c) in comparison to scenario b) due to the increase in ζ_{AP}. This shows the potential of integrating RIS to a D-MIMO system. Even though, the declining rate of η for case iii) of the D-MIMO system was large, the obtained η values were still better

than that for case i) of the MIMO system until a certain value of N_{RIS} for scenarios b) and c). The obtained results show the advantages of a D-MIMO system over a MIMO system and the improvement in η obtained with the integration of RIS to these systems.

E. Service coverage probability analysis of RIS-assisted D-MIMO system

In this analysis, the service coverage probability χ is analyzed for both RIS-integrated MIMO and D-MIMO system w.r.t. N_{RIS} range 1 to 256 to compare the variation in performance. For the D-MIMO system, two cases i) ζ_{AP} = 2 and ii) ζ_{AP} = 3 were considered. The analysis results are shown in Fig. 5.

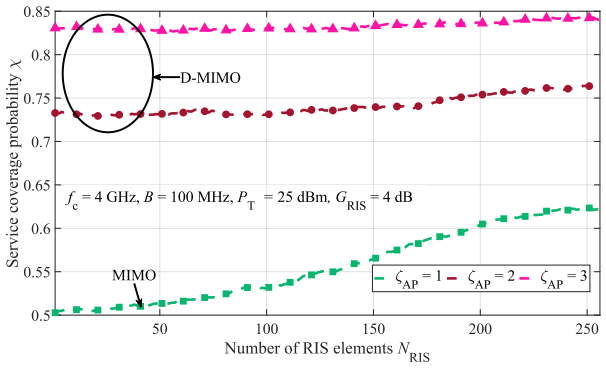

Fig. 5: Service coverage probability analysis w.r.t. the number of RIS elements for MIMO and D-MIMO models.

From this graph, it can be observed that there is a rise in χ in both MIMO and D-MIMO systems as we vary over the N_{RIS} range. The increasing rate of χ for the D-MIMO system is slow with an improvement of about 3% and 1% between the least and maximum value of the N_{RIS} range corresponding to cases i) and ii) respectively. Meanwhile, the increasing rate is significantly larger for the MIMO system compared to the D-MIMO system with an enhancement gap of about 12%. Even though this gap in the D-MIMO system with case i) is lower compared to the MIMO system, the service coverage in this D-MIMO system is 23% and 14% higher than that of the MIMO system at the lowest and highest value of the N_{RIS} range. This shows the advantage of the D-MIMO system over the MIMO system in terms of χ due to the multi-AP serving scenario present in the D-MIMO system. Also, the χ gets improved further as the size of the supporting RIS increases. The D-MIMO system with case ii) also shows an additional enhancement of 10% and 8% at the least and most N_{RIS} when compared to the D-MIMO system with case i) due to the presence of an additional serving AP in case ii) than case i). From these results, it can be concluded that the RIS is capable of enhancing the χ of the D-MIMO system. Also, this enhancement can be further improved by increasing N_{RIS} of the RIS-assisted D-MIMO system.

IV. Conclusions

In this paper, we considered a D-MIMO indoor system model with high UE density to which we integrated RIS to study the performance improvement of the system. An alternating optimization algorithm was adopted for the joint precoding optimization in a multi-AP serving scenario. Fair scheduling and queue-based approaches were utilized to serve the UEs in the system efficiently. Here, we considered different AP cluster sizes for serving the UEs in a D-MIMO system and found AP cluster sizes 2 and 3 to be the optimal choices based on the median SINR experienced by the UEs.

The results obtained from the average energy efficiency and service coverage analysis show the potential of integrating passive RIS in an indoor D-MIMO system for achieving a significant improvement in the average energy efficiency and service coverage even by utilizing a smaller number of RIS elements. This study also proves the positive impact that integration of RIS can bring in an indoor D-MIMO system by being an energy-efficient alternative to utilizing additional APs for improving the system performance. Future research includes the study of partitioned RIS for simultaneous and independent serving of multiple UEs which requires self-interference mitigation strategies to be investigated.

References

[1] O. Haliloglu et al., "Distributed MIMO Systems for 6G," 2023 Joint European Conference on Networks and Communications & 6G Summit (EuCNC/6G Summit), Gothenburg, Sweden, 2023, pp. 156–161.

[2] J. Sang et al., "Coverage Enhancement by Deploying RIS in 5G Commercial Mobile Networks: Field Trials," in IEEE Wireless Communications, vol. 31, no. 1, pp. 172–180, February 2024.

[3] T. S. Rappaport, Y. Xing, G. R. MacCartney, A. F. Molisch, E. Mellios and J. Zhang, "Overview of Millimeter Wave Communications for Fifth-Generation (5G) Wireless Networks—With a Focus on Propagation Models," in IEEE Transactions on Antennas and Propagation, vol. 65, no. 12, pp. 6213–6230, Dec. 2017.

[4] 3GPP TR 38.901 version 16.1.0 Release 16, 5G; Study on channel model for frequencies from 0.5 to 100 GHz.

[5] W. Wang and E. S. Lohan, "Applicability of 3GPP Indoor Hotspot Models to the Industrial Environments," 2018 8th Int. Conf. on Localization and GNSS (ICL-GNSS), Guimaraes, Portugal, 2018, pp. 1–5.

[6] A. Zappone, M. Di Renzo, F. Shams, X. Qian and M. Debbah, "Overhead-Aware Design of Reconfigurable Intelligent Surfaces in Smart Radio Environments," in IEEE Transactions on Wireless Communications, vol. 20, no. 1, pp. 126–141, Jan. 2021.

[7] F. Zhu, Y. Zhao, W. Xu and X. You, "CSIT-Free Model Aggregation for Multi-RIS-Assisted Over-the-Air Computation," 2022 Int.Symp. on Wireless Commun. Systems (ISWCS), Hangzhou, China, 2022, pp. 1–5.

[8] Q. Ye, O. Y. Bursalioglu, H. C. Papadopoulos, C. Caramanis and J. G. Andrews, "User Association and Interference Management in Massive MIMO HetNets," in IEEE Transactions on Communications, vol. 64, no. 5, pp. 2049–2065, May 2016.

[9] E. Björnson and L. Sanguinetti, "Scalable Cell-Free Massive MIMO Systems," in IEEE Transactions on Communications, vol. 68, no. 7, pp. 4247–4261, July 2020.

[10] Z. Li, H. Hu, J. Zhang and J. Zhang, "Enhancing Indoor mmWave Wireless Coverage: Small-Cell Densification or Reconfigurable Intelligent Surfaces Deployment?," in IEEE Wireless Communications Letters, vol. 10, no. 11, pp. 2547–2551, Nov. 2021.

[11] A. Zappone and M. Di Renzo, "Energy Efficiency Optimization of Reconfigurable Intelligent Surfaces With Electromagnetic Field Exposure Constraints," in IEEE Signal Proc. Letters, vol. 29, pp. 1447–1451, 2022.

[12] C. Huang, A. Zappone, G. C. Alexandropoulos, M. Debbah and C. Yuen, "Reconfigurable Intelligent Surfaces for Energy Efficiency in Wireless Communication," in IEEE Transactions on Wireless Communications, vol. 18, no. 8, pp. 4157–4170, Aug. 2019.

[13] J. Wang, W. Tang, S. Jin, X. Li and M. Matthaiou, "Static Power Consumption Modeling and Measurement of Reconfigurable Intelligent Surfaces," 2023 31st European Signal Processing Conference (EUSIPCO), Helsinki, Finland, 2023, pp. 890–894.